Carbon Nanotube-Based Supercapacitors with Excellent ac Line Filtering and Rate Capability *via* Improved Interfacial Impedance

Yverick Rangom, Xiaowu (Shirley) Tang,* and Linda F. Nazar*

Department of Chemistry and the Waterloo Institute for Nanotechnology, University of Waterloo, 200 University Avenue West, Waterloo, Ontario N2L 3G1, Canada

ABSTRACT We report the fabrication of high-performance, self-standing composite sp^2-carbon supercapacitor electrodes using single-walled carbon nanotubes (CNTs) as conductive binder. The 3-D mesoporous mesh architecture of CNT-based composite electrodes grants unimpaired ionic transport throughout relatively thick films and allows superior performance compared to graphene-based devices at an ac line frequency of 120 Hz. Metrics of 601 μF/cm^2 with a $-81°$ phase angle and a rate capability (RC) time constant of 199 μs are obtained for thin carbon films. The free-standing carbon films were obtained from a chlorosulfonic acid dispersion and interfaced to stainless steel current collectors with various surface treatments. CNT electrodes were able to cycle at 200 V/s and beyond, still showing a characteristic parallelepipedic cyclic votammetry shape at 1 kV/s. Current densities are measured in excess of 6400 A/g, and the electrodes retain more than 98% capacity after 1 million cycles. These promising results are attributed to a reduction of series resistance in the film through the CNT conductive network and especially to the surface treatment of the stainless steel current collector.

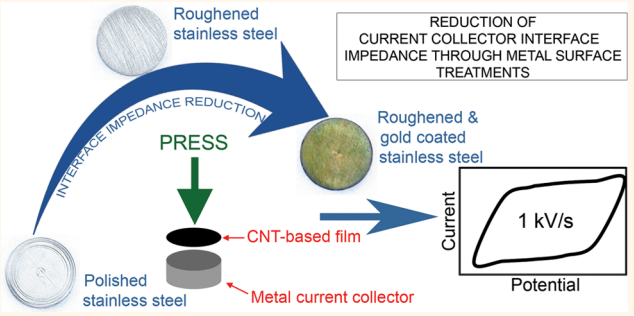

KEYWORDS: supercapacitor · EDLC · electric double layer capacitor · electrochemical capacitor · high current density · ultrahigh sweep rate · carbon nanotubes · ac line filtering

Electrochemical double-layer capacitors (EDLCs) are electrical devices which store energy by forming a double layer on their electrode/electrolyte interfaces. Since the charges are stored on a high surface area without any faradaic reaction involved, long cycle life can be obtained in addition to high capacitance. Moreover, EDLCs are vastly superior in terms of power density when compared against the current energy storage benchmark, Li-ion batteries.[1] These characteristics have allowed EDLCs, also known as "supercapacitors", to find important applications in electronics, industrial processes, and transportation where they support batteries and in a few cases replace them.[2,3]

High-frequency applications, such as 120 Hz ac line filtering, have thus far been dominated by electrolytic capacitors with a reduced capacitance compared to EDLCs. Traditional EDLCs take advantage of the very high surface area of activated carbons, where values greater than 1500 m^2/g are not uncommon. However, the convoluted ion paths in activated carbon cause the electrode to behave like a multiple time constant truncated ladder network.[4] As a result, the frequency response of traditional supercapacitors has been poor above 1 Hz, and they behave like pure resistors with impedance phase angles of nearly 0° at 120 Hz. In recent years, EDLC electrodes with vertically aligned graphene sheets have been reported that display a $-85°$ phase angle at 120 Hz.[5] This value is very close to ideal capacitor behavior where current trails voltage by $-90°$ in the complex plane representation for sinusoidal waves. All capacitors will display some resistive behavior whether from ionic or electronic sources and will only approach the ideal value at low frequency. At $-45°$, resistance and reactance contributions are equal; therefore, the frequency at this point is routinely used for comparing devices. The vertically aligned

* Address correspondence to lfnazar@uwaterloo.ca, tangxw@uwaterloo.ca.

Received for review April 7, 2015 and accepted June 5, 2015.

Published online June 05, 2015
10.1021/acsnano.5b02075

graphene sheets were obtained by either growing or reducing electrically conductive graphene directly onto metal current collectors. The resultant vertical nanoarchitecture provides excellent graphene−metal contact and good ionic transport.[5−7] Unfortunately, despite their high gravimetric energy density, graphene-based supercapacitors have low volumetric energy density, which limits their capacitance per unit area. This is because stacked sheets, even vertically stacked, often exhibit limited ionic transport. Other sp^2-carbon architectures may provide fast cycling with higher practical energy densities. Carbon nanotubes (CNTs) exhibit excellent electrical conductivity, and facile ionic (mass) transport can be optimized by the natural occurrence of mesostructured mesh-like frameworks when CNTs are stacked. These frameworks present a large surface area free of convoluted pores that minimize charge redistribution allowing the retention of full charge storage capacity at higher frequencies than porous carbons (PCs) or graphene alone.[8−11] Composite films of different carbons have been pursued in the past in an effort to combine complementary strengths. For example, CNTs and graphene composite have been shown to demonstrate good ionic conductivity and high volumetric energy density, and the addition of CNTs to PCs was reported to improve electrical conductivity.[12−14] However, the electrical conductivity of CNT mesostructured frameworks is often compromised by the dispersion methods used in their synthesis so that effective 120 Hz operation has been hindered to date.[15−18]

Here we report a versatile hybrid carbon electrode construction method that reduces equivalent series impedance and endows CNT-based macro-sized devices with ac line-filtering capabilities. We accomplished this by creating a dispersion that preserves the conductivity of single-walled CNTs while creating the required mesostructured network film and by attaching these films onto specially tailored current collectors. Aside from imparting good electrical conductivity, single-walled CNTs are simultaneously used as a highly conductive binder for other sp^2 carbons. We employed non-permanently functionalizing chlorosulfonic acid dispersion and filtration techniques, reported, respectively, by Pasquali *et al.* and Hetch *et al.* for graphene and CNTs, and applied these to mixtures of different sp^2 carbons.[19−22] The resulting mesostructured carbon films were free from the inherent areal capacitance limitations experienced by graphene-based devices. Films were then pressed onto polished, roughened, and/or gold-coated stainless steel current collectors to study the effect of specific collector surface treatment and ultimately minimize interface impedance. This study sheds light on the largely unexplored and critical role of creating extensive contact points between metal current collectors and the dry, binder-free, self-standing active materials increasingly used in high-power supercapacitor and battery applications.[23−25] Ultimate charge-transfer abilities were dependent on surface chemistry and roughness at the current collector/carbon interface, based on determination of comparison of the electrochemical properties.

RESULTS AND DISCUSSION

From the complex impedance representation, all 15 SWNT-MWNT (S-MW/NT) cells displayed the same electrolyte (ionic) real impedance contribution: 0.36 Ω with a standard deviation of 0.04 Ω. This constant ionic contribution regardless of film thickness was proof of good ionic mobility within these CNT films. Electronic impedance contributions differed significantly, however, depending on the choice of current collector as shown on Figure 1. A gold coating eliminates electronic impedance regardless of film thickness (Figure S3, Supporting Information). This proves that electronic impedance is not generated within the film but by the contact at the metal/carbon interface. These results are consistent with previous studies by Simon *et al.* on activated aluminum and on titanium/gold current collectors.[26,27] Chemical surface analysis through XPS and physical surface analysis through

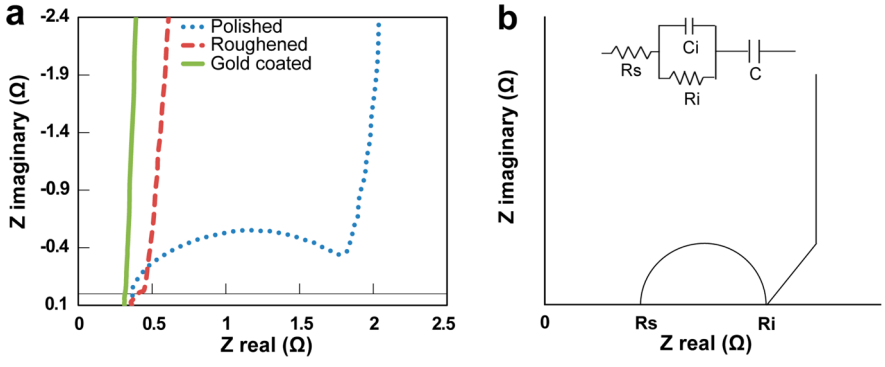

Figure 1. Impedance spectroscopy of a single walled−multiwalled carbon nanotube film (138 μg/cm^2; 0.5 M K_2SO_4) for polished, roughed, and gold-coated stainless steel current collectors: (a) complex plane impedance; (b) schematic showing equivalent circuit and complex plane impedance (R_s: solvent or ionic impedance, R_i: internal or electronic impedance, C_i: capacitance from contact resistance, R: additional resistance, C: EC capacitance)).

microprofilometer and AFM testing (Figure S11, Supporting Information) revealed that the roughened stainless steel surface bears more oxide than the polished one. Therefore, the performance advantage of the roughened surface could be attributed to an increased number of contact points between metal and carbon films. The roughened gold surface had no detectable oxide layer; scanning electron micrographs (SEM) of the surface exhibited nanoscale features that further increase effective contact with the carbon films.

Assuming a resistor−capacitor in series configuration ($C = -1/(2\pi f Z_{Im})$), the 138 μg/cm^2-S-MW/NT film (Figure 2) coupled with gold-coated current collectors in 0.5 M K_2SO_4 yielded an areal capacitance of 2087 μF/cm^2 at 120 Hz with a phase angle of −61° (Figure 3). Although the latter phase angle response suggests non-negligible resistance behavior, rendering this material poor for ac line-filtering applications, the available capacitance was seven times higher than vertically oriented graphene prepared from electrochemically reduced graphene oxide reported by Shi *et al.*,[6] and with a similar time constant (1.06 ms). The rate capability (RC) time constants characterize every capacitor and are the results of charge mobility limitations, electronic and ionic, which appear as compounded resistance in series with the main capacitance. Reduction of the time constant arises from minimizing the resistance in order to maintain significant high capacitance. Accordingly, the 19.9 μg/cm^2 SWNT thin film bonded to a gold-coated collector, cycled in a 0.5 M H_2SO_4 electrolyte, exhibited a proportionally much smaller 199 μs RC time constant that was similar to Miller's vertically oriented graphene electrodes, but with over two times the capacitance.[5,6,28] At 120 Hz, the measured capacitance was 601 μF/cm^2 at −81°, and the phase angle dropped to −45° at 1425 Hz (Figure 3). This represents a 2-fold increase in frequency response over the closest equivalent CNT-based device.[29] A summary of ultrahigh-rate capable aqueous supercapacitors and their performance is presented in Table 1. The performance displayed by our 19.9 μg/cm^2-SWNT thin-film capacitor makes it suitable for ac line-filtering applications, where standard 60 Hz ac power is rectified to an all-positive 120 Hz signal and then filtered to obtain dc power. Its reduced 199 μs time constant provides access to more than 95% of the energy storage in the charge/discharge time at 120 Hz.

According to the definition of capacitance, $C = q/V = (I/(\text{sweep rate}))$, the cyclic voltammetry (CV) sweep rate should remain proportional to current for an ideal constant capacitance. The 19.9 μg/cm^2-SWNT thin film mounted on gold-coated collectors and cycled in a H_2SO_4 electrolyte supported CV sweep rates up to at least 200 V/s while maintaining direct proportionality between sweep rate and discharge current (Figure 4). A parallelepiped shape was even maintained at 1 kV/s. This is a faster sweep rate than any macro-sized CNT-based supercapacitor and second to a reported graphene device which sustains proportional cycling sweep rates up to 350 V/s,[6] although these latter electrodes exhibit much lower capacitance per unit area than CNT films.[6,28,30−32] At the ultrahigh sweep rate of 200 V/s, the discharge current density reached 6400 A/g, which is an extremely high response.

At 200 V/s, S-MW/NT films mounted on gold collectors maintained quasiconstant current density values regardless of carbon loading, but the same films mounted on roughened and polished stainless steel

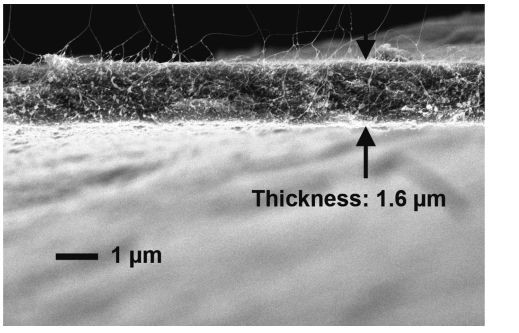

Figure 2. SEM image showing a cross-section of a 138 μg/cm^2-S-MW/NT film at 10000× magnification.

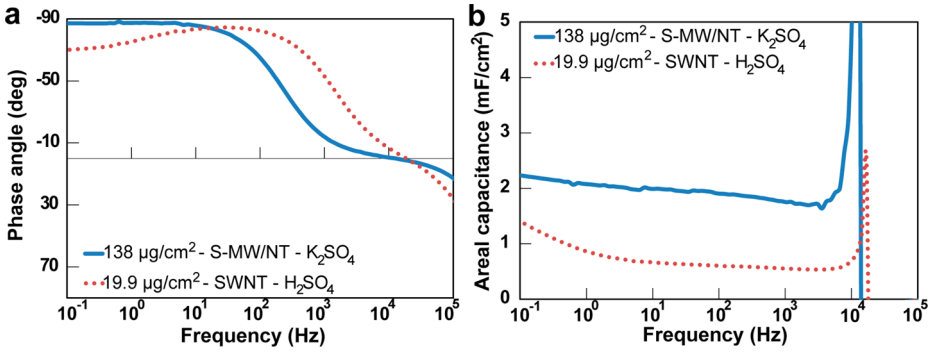

Figure 3. Frequency response of S-MW/NT and SWNT films: (a) phase angle *vs* frequency for a 19.9 μg/cm^2-SWNT film on a gold-coated stainless steel electrode (0.5 M H_2SO_4) and a 138 μg/cm^2-S-MW/NT film on gold-coated electrode (0.5 M K_2SO_4); (b) areal capacitance *vs* frequency.

TABLE 1. Comparison of High-Rate Capable Supercapacitors and Their Performance Metrics

	max specific capacitance (F/g)	max areal capacitance (μF/cm^2)	max scan rate (V/s)	frequency at −45° phase angle (Hz)	RC time constant at 120 Hz (μs)	areal capacitance at 120 Hz (μF/cm^2)	cycle life	ESR (Ω/cm^2)
vertically grown graphene[28]		187.5		15000	192.5	87.5		0.55
high density vertically grown graphene[5]				30000	251	94.8		1.65
electrochemically reduced graphene oxide[6]		325	350	4200	1350	283	10000—no loss	1.13
fiber-shaped EC reduced graphene oxide[7]		726	10		540		2000—6% loss	0.92
carbon onion microsupercapacitor[30]		900	100				10000	
3D graphene—CNT microsupercapacitor[6]		2160	400	500—1300	195—402	230—662		380—553
on-chip CNT supercapacitor[11]		200	2000	450				0.16
electrophoretic deposited CNT[29]	21		1	~600				1.17
CNT-sponge supercapacitor[38]	3.75	900	8				100000—2% loss	~6
carbon black thin film on vinyl[39]				641	354	559		0.3
carbon black thin film by inkjet printing[39]		500		764	588	120		4.9
SWNT	**27**	**600**	**200**	**1425**	**199**	**601**		**0.25**
S-MW/NT	**33**	**2300**	**100**	**223**	**1060**	**2087**	**1 million—<2%**	**0.3**
SWCNT-porous carbon	**100**	**11500**	**20**				**1 million—<2%**	**0.35**

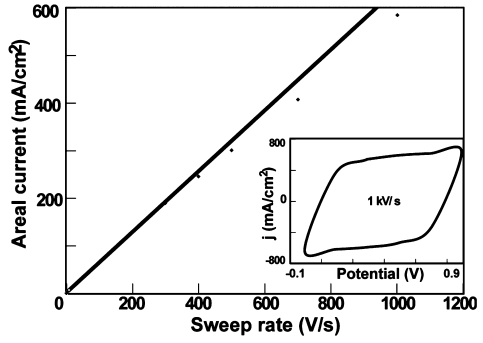

Figure 4. Cyclic voltammetry studies of a 19.9 μg/cm^2 SWNT film on a gold-coated stainless steel electrode (0.5 M H_2SO_4): discharge areal current *versus* scan rate showing onset of deviation from a linear response at 400 V/s (inset, CV at 1000 V/s).

collectors did not. For the latter only, current values leveled off at a maximum of about 160 mA/cm^2 even if carbon loadings were increased. That current maximum was the limiting factor for capacitance, singling out the carbon-metal interface as the bottleneck for charge transfer (Figure S4, Supporting Information).

Figure 5 shows the capacitance loss when 138 μg/cm^2-S-MW/NT-based cells were cycled from 1 to 100 A/g for 10000 cycles. Losses tend to disappear for current density values higher than 50 A/g. All S-MW/NT and SWNT-porous carbon cells could perform 1 million cycles with an average capacitance loss of 1.4% irrespective of current collector (observed maximum of 2.5%). The highest reported cycle life for EDLC devices typically vary between 10000 cycles for Shi's graphene-based device[6] and 100000 cycles for Cui's CNT design.[38] Impedance characteristics remained identical to pre-cycling values (Figure S7, Supporting Information). Loss percentage figures were the same regardless of the type of current collector used. Specific capacitance was measured to be 39 F/g for the 19.9 μg/cm^2-SWNT film, 33 F/g for S-MW/NT films, and 100 F/g for SWNT-porous carbon films with 0.5 M K_2SO_4 electrolyte. Carbon loadings from 19.9 to 138 μg/cm^2 do not affect specific capacitance for S-MW/NT films (Figure 6). Such maximum capacitance values are common for pure CNTs arranged in random networks. The superior capacitance of porous carbons is due to their larger specific surface area arising from multiple surface pores that contribute more than the single central pore of CNTs (Table 2).[33,34] It has been shown that capacitance contributions from surface-functionalized groups decrease as frequencies, which are proportional to current density, increase past a few hertz.[15] Our carbons have not been intentionally functionalized, and this was verified using FTIR characterization (Figure S1, Supporting Information). Some functionalized groups may form naturally from oxidation during production, however, and even when carbon is left in storage in air. The observed dependence of capacitance loss on current density values may then be explained by the suppression of pseudocapacitance contributions from carboxyl or carboxylic groups at higher cycle frequencies.

Galvanostatic tests on a cell with SWNT loading scaled up 20-fold to 2830 μg/cm^2 revealed that specific capacitance is maintained. This result confirms that the full surface area of the CNTs remains accessible to ions independently of carbon loading. Cyclic voltammetry tests of these 2.83 mg/cm^2 electrodes reveal near-ideal behavior up to 1 V/s (Figure 7a), which demonstrates that adequate ionic pathways are maintained. The Nyquist plot (Figure 7b) compares the impedance response from thin and thick electrodes, showing that the high-loading thick electrodes diverge from ideal capacitor behavior at high frequencies as well as suffer from slightly higher ionic impedance when compared to thin electrodes. The absence of a semicircle component attests to good electronic conductivity both throughout the carbon and at the current collector

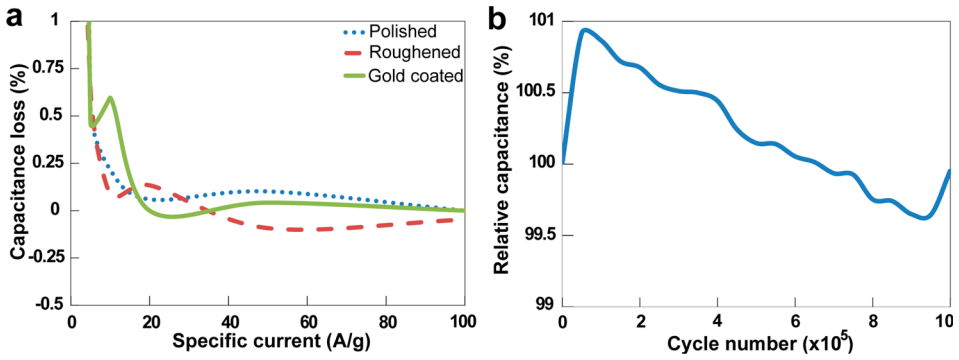

Figure 5. Galvanostatic discharge tests of 138 μg/cm^2 S-MW/NT films in 0.5 M K_2SO_4 aqueous electrolyte: (a) capacitance loss *vs* current density for polished, roughened, and gold-coated stainless steel current collector; (b) plot of capacitance retention over a 1 million cycles on a gold-coated collector cycled at 200 A/g.

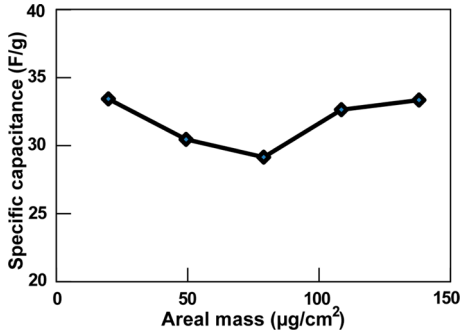

Figure 6. Cyclic voltammetry study of S-MW/NT films of various carbon loadings showing specific capacitance *vs* mass per surface area (20 V/s; 0.5 M K_2SO_4; gold-coated stainless steel current collector).

TABLE 2. BET Specific Surface Area Measurements of sp^2-Carbon Films

	specific surface (m^2/g)	avg pore size (nm)
SWNT	510	5.6
S-MW/NT	352	6.5
SWNT-porous carbon	900	3.8

interface. However, the frequency response was poorer in the thick CNT films as expected: full specific capacitance was maintained only up to about 10 Hz with a phase angle dropping below −45° (Figure 7c,d). The loss of frequency response is undoubtedly due to ion diffusion limitations.

The graphene-based devices produced by Miller[5] and Shi[6] exhibit the same lack of electronic impedance contributions undetectable through EIS as our CNT-based electrodes using gold-coated current collectors. They presented lower overall capacitance but higher frequency response, in fact, the highest reported frequency response for supercapacitors (Table 1). The direct growth and bonding used in Miller's and Shi's reports appear to be key contributors to enabling reliable fast cycling and improved high frequency response. Miller's fabrication method leads to effective, durable, and relatively cheap excellent contact at the interface of carbon and current collector. Graphene also has a more natural ability to form extensive contact with a relatively flat surface than do carbon nanotubes, due to its sheetlike morphology. Furthermore, graphene grown at 1000 °C directly on a nickel substrate results in a temperature high enough to induce atomic interdiffusion of carbon into nickel, which is speculated to form very effective metallic carbide channels to allow electrons to easily cross the carbon/metal interface.[35] However, CVD is unlikely to be a practical method for scaled up commercial production. Nevertheless, following Miller's lead, designs of energy storage devices may soon include bonding techniques developed decades ago in solar cell technologies where metal current collectors are interfaced to active material through atomic diffusion to create low-resistance, energy-efficient heterojunctions.[36] Contact of our electrodes only relies on static friction between relatively expensive gold-coated current collectors and the CNT-based carbon films. Further improvement of contacts will be the subsequent focus of our work.

CONCLUSIONS

In this study, the rate capability of well-known sp^2-carbon compounds have been demonstrated to be at least 2 orders of magnitude higher than previously reported: 2000 A/g for SWNT/porous carbon films, 2400 A/g for S-MW/NT films, and 6400 A/g for SWNT films. These high current densities are enabled by the self-assembly of the CNTs into flexible mesostructured networks incorporating other sp^2-carbons that are favorable for both ionic and electron transport and by decreasing impedance at the current collector interface. Our versatile method allows the fabrication of electrodes that compete well with graphene-based EDLCs, displaying low interfacial resistivity, higher areal capacitance, and much improved reported cycle life. The ac line-filtering applications are now within reach of CNT-based supercapacitors.

We have also demonstrated that, for mesostructured electrodes with unimpaired ionic transport abilities, frequency response limitations arise primarily from

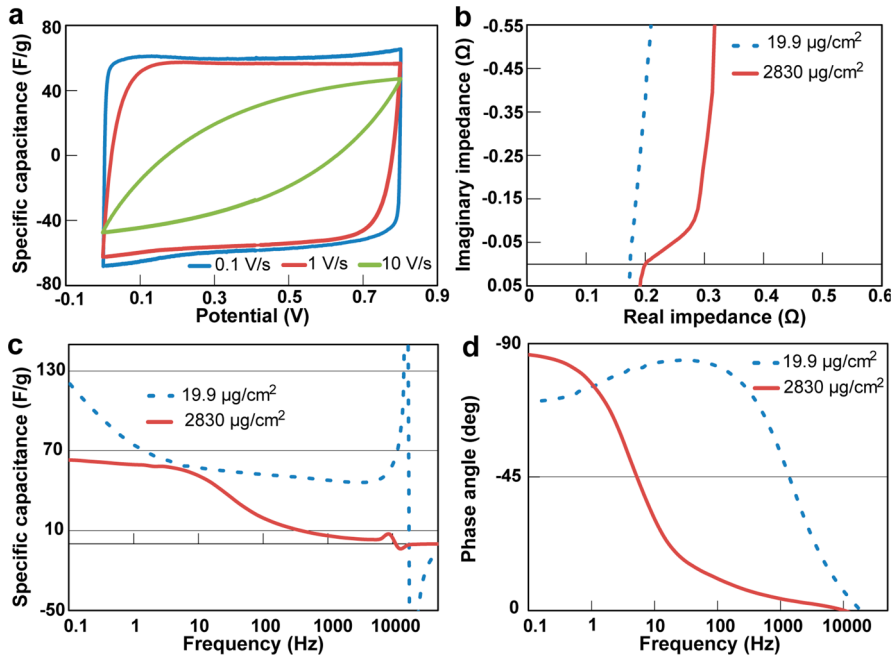

Figure 7. (a) Cyclic voltammetry study of 2830 μg/cm^2 SWNT film on gold-coated current collectors (0.5 M H_2SO_4) showing specific capacitance *versus* potential at different sweep rates: 0.1 V/s (blue), 1 V/s (red), and 10 V/s (green). (b) Nyquist plot comparing low loading (19.9 μg/cm^2) to high loading (2830 μg/cm^2) films; frequency response of 19.9 and 2830 μg/cm^2 SWNT films on gold-coated collector (0.5 M H_2SO_4). (c) Specific capacitance *versus* frequency. (d) Phase angle *versus* frequency.

electronic transfer through the carbon/metal interface. This indicates that better interface conductivity is still a key component in future developments of high-power energy storage devices. Further experiments and studies of charge transfer at the current collector interface will certainly help reduce series impedance further and increase energy efficiency beyond EDLC applications. We foresee improvements arising from deliberately inducing compositionally seamless interface gradients between carbon and metal collectors. Nevertheless the electrode construction technique presented here is readily applicable for improving the growing number of free-standing, binder-free applications that rely on carbons for electronic transport.

METHODS

Binder-Free Carbon Films, Electrode, and Cell Preparation. Single and hybrid carbon films were made by combining the methods of Pasquali *et al.* for dispersion and of Hecht *et al.* for filtration.[19−22] CNTs and Ketjenblack carbon were dispersed in 99% chlorosulfonic acid (CSA, Sigma-Aldrich) and stirred overnight, and then the colloidal dispersions were vacuum-filtered through alumina filters (Whatman) with pores of different diameters: 0.02 μm for SWNT films (Figure S2a, Supporting Information), 0.1 μm for S-MW/NT films (Figure 2 and Figure S2b), and 0.2 μm for SWNT-porous carbon films (Figure S2c). Films were rinsed with chloroform (>99.8%, Sigma-Aldrich) before a DI−water bath was used to float off the hydrophobic films and separate them from the filters. SWNT films were filtered from a 0.33 mg/mL CSA dispersion. S-MW/NT films were made from five CSA dispersions with concentrations ranging from 0.33 to 1.67 mg/mL. The ratio SWNTs to MWNTs was 10−90 wt %. SWNT−porous carbon films were prepared from two dispersions with concentrations of 1.67 and 3.33 mg/mL, 20 wt % SWNT to 80 wt % PC. The resulting films had masses per unit area from 19.9 to 288 μg/cm^2. CNTs were purchased from Cheaptubes and used without further purification. These tubes comprised 99 wt % SWNTs ranging from 1 to 2 nm diameter that are <30 μm long and 95 wt % MWNTs, <8 nm in diameter, and <30 μm long.

Accurate mass determination is critical to the characterization of film performance, namely specific capacitance, and current densities. The masses involved are very small, and losses occurred during filtering, as a result, final films were lighter than expected. Final mass determination was carried out using a thermogravimetric analyzer (TA Instruments Q600) with sub-microgram accuracy. The process is destructive: sp^2 carbon combusts completely in air below 400 °C. Accurate measurement of the carbon content in each carbon loading film was obtained from the mass difference before and after combustion, averaged over five samples using a linear fit. For SWNT−porous carbon films, the same technique was employed. However, since only two thicknesses were needed, it was not possible to rely on a linear fit. Instead, four films were combusted, two samples for each thickness, and an average weight was calculated for each film.

Using a Carver press, films were interfaced directly to 318 stainless steel metal current collector rods with three different surface finishes: machined polished, roughened, and gold coated. Roughened rods were obtained by scratching machine polished rods with P100 aluminum oxide and paper. Gold-coated rods were produced by sputtering a ~20 nm thick layer of gold onto roughened rods. The pressure exerted between film and collector was 98 MPa for all fabricated electrodes. All rods were 1.2 cm diameter cylinders that could be used directly in two-electrode type Swagelok cell apparatuses. The SWNT films and SWNT-porous carbon films were exclusively interfaced to gold-coated collectors; S-MW/NT films were cycled using all three collector surface finishes.

All cells consisted of symmetrical full cells with identical electrodes (carbon film + current collector) on either side. Two different aqueous electrolytes were utilized: (i) potassium

sulfate (K_2SO_4) at 0.5 M concentration in Milli-Q purified water with 18 MΩ.cm resistivity; (ii) concentrated 98% sulfuric acid (H_2SO_4) diluted in Milli-Q water to 0.5 M. Fiber glass prefilters from Millipore were soaked in the electrolyte and placed between the electrodes to serve as separators.

Eighteen cells were tested:

(1) Two SWNT-based cells interfaced with gold-coated current collectors, one with a low carbon loading of 19.9 μg/cm^2 and one with a high carbon loading of 2830 μg/cm^2 with 0.5 M H_2SO_4 as the electrolyte in both cases.

(2) Two SWNT-porous carbon-based cells of two different carbon loadings (148.0 and 288 μg/cm^2) interfaced to gold-coated collectors with 0.5 M K_2SO_4 as the electrolyte.

(3) Fifteen S-MW/NT-based cells with five different carbon loadings (19.9, 49.4, 78.9, 108.4, and 138.0 μg/cm^2) interfaced to all three types of collector with 0.5 M K_2SO_4 as the electrolyte.

Electrochemical Studies. Best practice methods were followed for measuring and deriving the electrochemical properties of supercapacitors.[37] All cells were tested using a Biologic VMP3 galvanostat, and data were analyzed with EC-lab software. Galvanostatic experiments were conducted with current density values from 1 to 1460 A/g between 0 and 0.8 V. Cyclic voltammetry sweep rates were varied from 0.1 to 1 kV/s; measurements above 200 V/s are only qualitative as the galvanostatic sampling frequency becomes insufficient for quantitative use above that sweep rate. Electrochemical impedance spectroscopy (EIS) measurements were conducted from 500 kHz to 100 mHz at a 5 mV amplitude with +0.1 V offset.

Surface Characterization. Microscale surface roughness was characterized with a Dektak 8 Stylus contact profilometer. The surface of each current collector was probed across a 200-μm horizontal travel distance. Vertical travel of the contact element was restricted to a maximum range of 6.5 μm, and 4.4 mg of weight was applied to keep contact with the sample.

AFM characterization was conducted on a MultiMode scanning probe microscope with Nanoscope controller from Digital Instrument Veeco Metrology Group. Each current collector surface was raster scan over 1 μm^2 area and averaged over 512 passes.

XPS measurements were conducted under high vacuum on a Thermo VG Scientific ESCALab 250 XPS microprobe system with a monochromatic Al Kα (1486.6 eV) 150 W X-ray source with 0.5 mm circular spot size.

Conflict of Interest: The authors declare no competing financial interest.

Acknowledgment. We thank the Natural Sciences and Engineering Council of Canada for generous financial support of this work through their Discovery and Canada Research Chair programs.

Supporting Information Available: FTIR and Raman studies of CNT before and after exposure to chlorosulfonic acid (Figure S1). Additional SEM images of all three types of films, additional comparative electrochemistry characterizations (CV, impedance spectroscopy) of CNT films of different thickness on different current collectors are shown in Figures S2–S8. XPS, surface profilometer analysis of metal current collectors, relative surface area approximation, and experimental error quantification (Figures S9–S12). The Supporting Information is available free of charge on the ACS Publications website at DOI: 10.1021/acsnano.5b02075.

REFERENCES AND NOTES

1. Gogotsi, Y.; Simon, P. True Performance Metrics in Electrochemical Energy Storage. *Science* **2011**, *334*, 917–918.
2. Simon, P.; Gogotsi, Y. Materials for Electrochemical Capacitors. *Nat. Mater.* **2008**, *7*, 845–854.
3. Miller, J. R.; Burke, A. F. Electrochemical Capacitors: Challenges and Opportunities for Real-World Applications. *Electrochem. Soc. Interface* **2008**, *17*, 53–57.
4. Miller, J. R. Introduction to Electrochemical Capacitor Technology. *IEEE Electr. Insul. Mag.* **2010**, *26*, 40–47.
5. Cai, M.; Outlaw, R. A.; Butler, S. M.; Miller, J. R. A High Density of Vertically-Oriented Graphenes for Use in Electric Double Layer Capacitors. *Carbon* **2012**, *50*, 5481–5488.
6. Sheng, K.; Sun, Y.; Li, C.; Yuan, W.; Shi, G. Ultrahigh-Rate Supercapacitors Based on Electrochemically Reduced Graphene Oxide for ac Line-filtering. *Scientific Rep.* **2011**, *2*, 247.
7. Li, Y.; Sheng, K.; Yuan, W.; Shi, G. A High-Performance Flexible Fibre-shaped Electrochemical Capacitor Based on Electrochemically Reduced Graphene Oxide. *Chem. Commun.* **2013**, *49*, 291–293.
8. Black, J.; Andreas, H. A. Effects of Charge Redistribution on Self-Discharge of Electrochemical Capacitors. *Electrochemica Acta* **2009**, *54*, 3568–3574.
9. Taberna, P.-L.; Portet, C.; Simon, P. Electrode Surface Treatment and Electrochemical Impedance Spectroscopy Study on Carbon/Carbon Supercapacitors. *Appl. Phys. A: Mater. Sci. Process.* **2006**, *82*, 639–646.
10. Frackowiak, E. Carbon Materials for Supercapacitor Application. *Phys. Chem. Chem. Phys.* **2007**, *9*, 1774–1785.
11. Dinh, T. M.; Armstrong, K.; Guay, D.; Pech, D. High-Resolution On-Chip Supercapacitors with Ultra-high Scan Rate Ability. *J. Mater. Chem. A* **2014**, *2*, 7170–7174.
12. Zhu, Y.; Murali, S.; Stoller, M. D.; Ganesh, K. J.; Cai, W.; Ferreira, P. J.; Pirkle, A.; Wallace, R. M.; Cychosz, K. A.; Thommes, M.; et al. Carbon-Based Supercapacitors Produced by Activation of Graphene. *Science* **2011**, *332*, 1537–1541.
13. Kim, T. Y.; Jung, G.; Yoo, S.; Suh, K. S.; Ruoff, R. S. Activated Graphene-Based Carbons as Supercapacitor Electrodes with Macro- and Mesopores. *ACS Nano* **2013**, *7*, 6899–6905.
14. Zhang, L. L.; Zhao, X.; Stoller, M. D.; Zhu, Y.; Ji, H.; Murali, S.; Wu, Y.; Perales, S.; Clevenger, B.; Ruoff, R. S. Highly Conductive and Porous Activated Reduced Graphene Oxide Films for High-Power Supercapacitors. *Nano Lett.* **2012**, *12*, 1806–1812.
15. Niu, C.; Sichel, E. K.; Hoch, R.; Moy, D.; Tennent, H. High Power Electrochemical Capacitors Based on Carbon Nanotube Electrodes. *Appl. Phys. Lett.* **1997**, *70*, 1480–1482.
16. Simon, P.; Gogotsi, Y. Charge Storage Mechanism in Nanoporous Carbons and Its Consequence for Electrical Double Layer Capacitors. *Philos. Trans. R. Soc. A* **2010B**, *368*, 3457–3467.
17. Tung, V. C.; Chen, L.-M.; Allen, M. J.; Wassei, J. K.; Nelson, K.; Kaner, R. B.; Yang, Y. Low-Temperature Solution Processing of Graphene–Carbon Nanotube Hybrid Materials for High-Performance Transparent Conductors. *Nano Lett.* **2009**, *Vol. 9*, 1949–1955.
18. Xu, Z.; Li, Z.; Holt, C. M. B.; Tan, X.; Wang, H.; Amirkhiz, B. S.; Stephenson, T.; Mitlin, D. Electrochemical Supercapacitor Electrodes from Sponge-like Graphene Nanoarchitectures with Ultrahigh Power Density. *J. Phys. Chem. Lett.* **2012**, *3*, 2928–2933.
19. Ramesh, S.; Ericson, L. M.; Davis, V. A.; Saini, R. K.; Kittrell, C.; Pasquali, M.; Billups, W. E.; Adams, W. W.; Hauge, R. H.; Smalley, R. E. Dissolution of Pristine Single Walled Carbon Nanotubes in Superacids by Direct Protonation. *J. Phys. Chem. B* **2004**, *108*, 8794–8798.
20. Behabtu, N.; Lomeda, J. R.; Green, M. J.; Higginbotham, A. L.; Sinitskii, A.; Kosynkin, D. V.; Tsentalovich, D.; Parra-Vasquez, A. N. G.; Schmidt, J.; Kesselman, E.; et al. Spontaneous High-Concentration Dispersions and Liquid Crystals of Graphene. *Nat. Nanotechnol.* **2010**, *5*, 406–411.
21. Davis, V. A.; Parra-Vasquez, A. N. G.; Green, M. J.; Rai, P. K.; Behabtu, N.; Prieto, V.; Booker, R. D.; Schmidt, J.; Kesselman, E.; Zhou, W.; Fan, H.; et al. True Solutions of Single-Walled Carbon Nanotubes for Assembly into Macroscopic Materials. *Nat. Nanotechnol.* **2009**, *4*, 830–834.
22. Hecht, D. S.; Heintz, A. M.; Lee, R.; Hu, L.; Moore, B.; Cucksey, C.; Risser, S. High Conductivity Transparent Carbon Nanotube Films Deposited from Superacid. *Nanotechnol.* **2011**, *22*, 075201.

23. Zhong, C.; Wang, J.-Z.; Wexler, D.; Liu, H.-K. Microwave Autoclave Synthesized Multi-Layer Graphene/Single-Walled Carbon Nanotube Composites for Free-Standing Lithium-Ion Battery Anodes. *Carbon* **2014**, *66*, 637–645.
24. Wang, R.; Xu, C.; Sun, J.; Liu, Y.; Gao, L.; Yao, H.; Lin, C. Heat-Induced Formation of Porous and Free-standing MoS_2/GS Hybrid Electrodes for Binder-Free and Ultralong-Life Lithium Ion Batteries. *Nano Energy* **2014**, *61*, 183–195.
25. Cheng, J.; Wang, B.; Xin, H. L.; Kim, C.; Nie, F.; Li, X.; Yang, G.; Huang, H. Conformal Coating of TiO_2 Nanorods on a 3-D CNT Scaffold by Using a CNT Film As a Nanoreactor: a Free-standing and Binder-Free Li-Ion Anode. *J. Mater. Chem. A* **2014**, *2*, 2701–2707.
26. Portet, C.; Taberna, P.-L.; Simon, P.; Laberty-Robert, C. Modification of Al Current Collector Surface by Sol−Gel Deposit for Carbon−Carbon Supercapacitor Application. *Electrochem. Acta* **2004**, *49*, 905–912.
27. Huang, P.; Heon, M.; Pech, D.; Brunet, M.; Taberna, P.-L.; Gogotsi, Y.; Lofland, S.; Hettinger, J. D.; Simon, P. Micro-Supercapacitors from Carbide Derived Carbon (CDC) Films on Silicon Chips. *J. Power Sources* **2013**, *225*, 240–244.
28. Miller, J. R.; Outlaw, R. A.; Holloway, B. C. Graphene Double-Layer Capacitor with ac Line-Filtering Performance. *Science* **2010**, *329*, 1637–1639.
29. Du, C.; Pan, N. Supercapacitors Using Carbon Nanotubes Films by Electrophoretic Deposition. *J. Power Sources* **2006**, *160*, 1487–1494.
30. Pech, D.; Brunet, M.; Durou, H.; Huang, P.; Mochalin, V.; Gogotsi, Y.; Taberna, P.-L.; Simon, P. Ultrahigh-Power Micrometre-Sized Supercapacitors Based on Onion-Like Carbon. *Nat. Nanotechnol.* **2010**, *5*, 651–654.
31. Lin, R.; Taberna, P.-L.; Chmiola, J.; Guay, D.; Gogotsi, Y.; Simon, P. Microelectrode Study of Pore Size, Ion Size, and Solvent Effects on the Charge/Discharge Behavior of Microporous Carbons for Electrical Double-Layer Capacitors. *J. Electrochem. Soc.* **2009**, *156*, A7–A12.
32. Sano, N.; Wang, H.; Chhowalla, M.; Alexandrou, I.; Amaratunga, G. A. J. Nanotechnology: Synthesis of Carbon "Onions" in Water. *Nature* **2001**, *414*, 506–507.
33. Zhao, X.; Chu, B. T. T.; Ballesteros, B.; Wang, W.; Johnston, C.; Sykes, J. M.; Grant, P. S. Spray Deposition of Steam Treated and Functionalized Single-Walled and Multi-Walled Carbon Nanotube Films for Supercapacitors. *Nanotechnology* **2009**, *20*, 065605.
34. Bao, Q.; Bao, S.; Li, C. M.; Qi, X.; Pan, C.; Zang, J.; Lu, Z.; Li, Y.; Tang, D. Y.; Zhang, S.; Lian, K. Supercapacitance of Solid Carbon Nanofibers Made from Ethanol Flames. *J. Phys. Chem. C* **2008**, *112*, 3612–3618.
35. Cai, M.; Outlaw, R. A.; Quinlan, R. A.; Premathilake, D.; Butler, S. M.; Miller, J. R. Fast Response, Vertically Oriented Graphene Nanosheet Electric Double Layer Capacitors Synthesized from C_2H_2. *ACS Nano* **2014**, *8*, 5873–5882.
36. Sundaresan, R.; Burk, D. E.; Fossum, J. G. Potential Improvement of Polysilicon Solar Cells by Grain Boundary and Intragrain Diffusion of Aluminum. *J. Appl. Phys.* **1984**, *55*, 1162–1167.
37. Stoller, M. D.; Ruoff, R. S. Best Practice Methods for Determining an Electrode Material's Performance for Ultracapacitors. *Energy Environ. Sci.* **2010**, *3*, 1294–1301.
38. Chen, W.; Rakhi, R. B.; Hu, L.; Xie, X.; Cui, Y.; Alshareef, H. N. High-Performance Nanostructured Supercapacitors on a Sponge. *Nano Lett.* **2011**, *11*, 5165–5172.
39. Kossyrev, P. Carbon Black Supercapacitors Employing Thin Electrodes. *J. Power Sources* **2012**, *201*, 347–352.